Numerical simulation of galvanized rebars pullout

H.F.S.G. Pereira
Engineering Department, School of Science and Technology, University of Trás-os-Montes e Alto Douro, Quinta de Prados, 5001-801 Vila Real, Portugal.
IDMEC, Pólo FEUP, Rua Dr. Roberto Frias, 4200-465 Porto, Portugal
hfpereira@portugalmail.pt

V.M.C.F. Cunha, J. Sena-Cruz
Department of Civil Engineering, School of Engineering, University of Minho 4800-058 Guimarães, Portugal.
ISISE, University of Minho 4800-058 Guimarães, Portugal

ABSTRACT. The usage of rebars in construction is the most common method for reinforcing plain concrete and thus bridging the tensile stresses along the concrete crack surfaces. Usually design codes for modelling the bond behaviour of rebars and concrete suggest a local bond stress – slip relationship that comprises distinct reinforcement mechanisms, such as adhesion, friction and mechanical anchorage. In this work, numerical simulations of pullout tests were performed using the finite element method framework. The interaction between rebar and concrete was modelled using cohesive elements. Distinct local bond laws were used and compared with ones proposed by the Model Code 2010. Finally an attempt was made to model the geometry of the rebar ribs in conjunction with a material damaged plasticity model for concrete.

KEYWORDS. Pullout Test; Local Bond; Damage; Finite Element Method.

INTRODUCTION

The first works associated to the study of the adherence between concrete and steel rebars, probably, were carried out by Considère in the end of the XIX century [1, 2]. After the latter works, several others were carried out regarding the experimental study of the bond between concrete and rebars, with special incidence in the decades of 70, 80 and 90 of the past century [3 - 19]. Within the two last decades, some numerical works about the bond behaviour between concrete and rebars were carried out, some with special incidence on the behaviour associated to pullout tests, e.g. [20 - 23], and others related to the bond behaviour in structural elements, e.g. [24].
Reinforced concrete can be regarded as a composite material made up of two components (steel and concrete) with rather distinct mechanical and physical properties. In general, due to the external loads applied to a structural concrete element will arise a certain stress field, being the tensile stresses after cracking bridged by the reinforcing rebars due to the bond mechanisms developed at the rebar / matrix interface. "Bond stresses" is the designation ascribed to the shear stresses that arise at the rebar / concrete interface. This bond stresses, when efficiently mobilized, enable the two materials to behave as a composite material. In concrete reinforced structures, the bond between the distinct components of the reinforced concrete member has a primordial role on the overall behaviour and if neglected can lead to poor structural

response. These complex phenomena involved in the bond behaviour have led engineers in the past to rely heavily on empirical formulas for the design of concrete structures, which were derived from numerous experiments, e.g. [7 - 15]. The properties of the adherence between rebar / matrix depends on several factors, such as friction, mechanical interaction and chemical adhesion [24].
In the past, several experimental investigations have been carried out in order to clarify and understand the behaviour of deformed bars pulled out from a concrete bulk under monotonic as well as cyclic loading conditions. Some of these experimental results are well documented in literature, e.g. [7-19, 25]. Based exclusively on the experimental results it is difficult to filter out the influences of material and geometrical parameters on the bond behaviour. In order to understand thoroughly the bond behaviour, a reliable numerical model (simulation of the transmission of forces at the interface zone, see Fig. 1a) should be employed, thus a three-dimensional finite element, analysis is needed. The numerical modelling of the bond behaviour is principally possible at two different levels: (1) detailed modelling (see Fig. 1b) in which the geometry of the bar and the concrete are modelled with three-dimensional elements and (2) phenomenological modelling (see Fig. 1c) based on a smeared or discrete formulation of the bar-concrete interface [21].

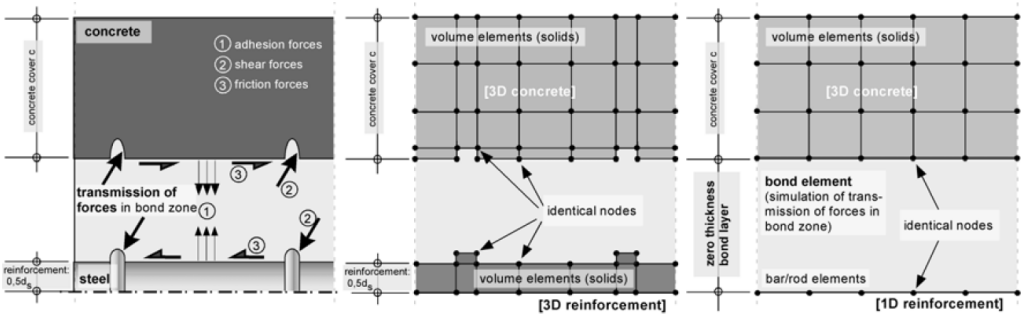

(a) Idealized bond zone. (b) Detailed modelling. (c) Phenomenological modelling.

Figure 1: Schematic simulation of the idealized bond zone [21].

The phenomenological modelling of bond between rebar / concrete can be discretised by three-dimensional finite elements. The link between the rebar and the concrete can be achieved by a discontinuous approach, where bond is defined by discrete or reduced thickness cohesive elements. Within these elements the behaviour is controlled by the local bond stress-slip relationship. This approach is able to realistically predict the pullout behaviour for different geometries and for different boundary conditions only if a realistic constitutive bond relationship is used. However, the model is not able to straightforwardly predict the bond behaviour of a given bar geometry. Consequently, the influence of these parameters must be stored in advance in the basic parameters matrix of the bond model. Thus, one has the possibility to realistically simulate the behaviour of reinforced concrete structures with relatively low effort in modelling and computing time. By the use of detailed modelling, such as both modelling of the ribs of the reinforcement and the concrete lugs (see Fig. 1b) between the ribs of the reinforcement a quite refined finite element mesh has to be generated. This leads again to a high effort in modelling, and also to really long computational time, in particular while carrying out a finite element analysis of complex reinforced concrete structures [21 - 23].
In the present work a parametric study of the numerical simulations of galvanized rebar pullout tests under the finite element framework is presented and discussed. Afterwards, the numerical simulations of galvanized rebar pullout tests are compared with the results obtained by using an analytical model [31], namely, a shear-lag model. The adopted local bond-slip laws were similar to the one proposed by the CEB-FIP Model Code 2010 [27]. Finally, an attempt is made to model the pullout tests by isolating the distinct bond mechanisms, in particular, the mechanical component of bond due to the rebar's ribs. Therefore, to fulfil this purpose a three-dimensional finite element model considering the geometrical modelling of the rebar ribs was implemented.

DESCRIPTION OF THE NUMERICAL MODEL

Geometry

The experimental pullout tests were carried out on concrete cubic specimens with a rebar positioned in the middle of the specimen. The rebar's embedded length was equal to half of the cube edge length, i.e. 100 mm, Fig. 2. Only one quarter of the experimental specimen was geometrically modelled, because the specimen has double symmetry

conditions. Fig. 3 shows the 3D geometrical model with the representation of the surfaces' boundary conditions ascribed due to both symmetry conditions and test support conditions. The perpendicular displacements of the finite element nodes at the two symmetry planes were constrained along the *yy* and *zz* axis, respectively. Moreover, at the specimen's front plane (where the protruding end of the rebar arises), the displacement of the nodes perpendicular to the plane were also constrained, i.e. in the *xx* direction.

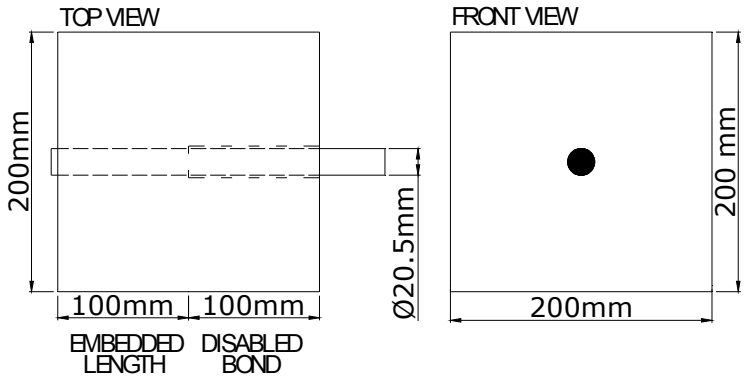

Figure 2: Geometry of the specimens used in the pullout test.

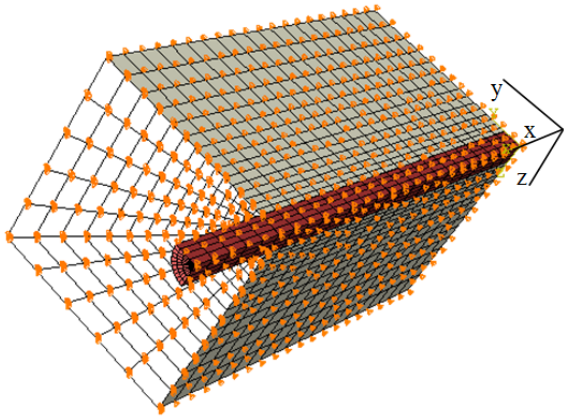

Figure 3: 3D FE mesh and boundary conditions.

The pullout specimen was modelled using 3D solid finite elements available from ABAQUS library [26], namely, C3D8 and C3D6 were used to model the concrete bulk and steel rebar, respectively. Additionally, cohesive elements (COH3D8) were considered to model the interface behaviour between the concrete and rebar.

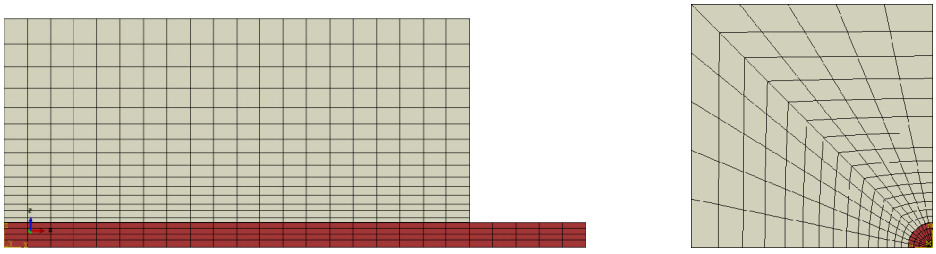

(a) (b)

Figure 4: Model with smooth rebar: a) top view, b) front view.

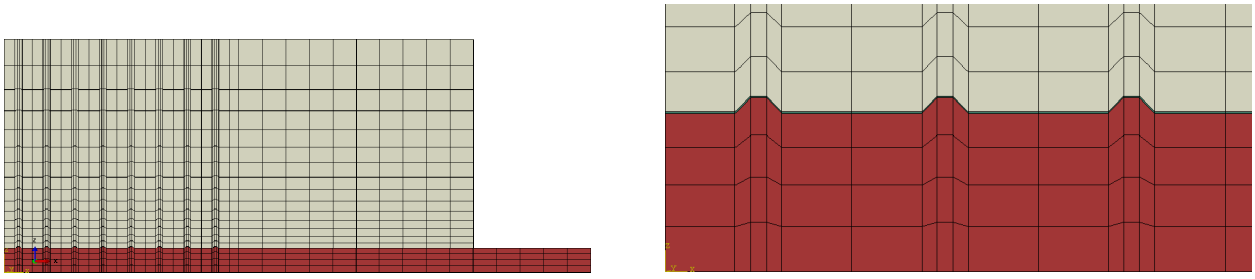

(a) (b)

Figure 5: Model with ribbing rebar: a) top view, b) ribbing detail.

Local bond-slip law

The bond properties of a reinforcing rebar can be analytically described by a local bond stress – slip relationship, $\tau = \tau(s)$, in which τ is the shear stress acting on the contact surface between rebar and concrete, and s is the corresponding slip, i.e. the relative displacement between steel bar and concrete [31]. Once the relation $\tau = \tau(s)$ is known, using equilibrium and compatibility relations, the second order differential equation governing the slip can be defined as:

$$\frac{d^2 s}{dx^2} - \frac{\pi D}{E_s A_s}\tau(s) = 0 \quad (1)$$

where D is the diameter, A_s is the cross sectional area, E_s is the Young's modulus of the reinforcing bars and $s(x)$ is the slip between concrete and the embedded rebar's length at the abscissa x. Using Eq. (1), important phenomena can be analysed such as: the anchorage length evaluation, the determination of the tension stiffening effect and crack spacing and opening. These problems can be solved once the boundary conditions of the specific problems are specified and this observation reinforces the importance of a consistent local bond-slip relationship.

Relatively to the analytical expressions for the bond-slip relationships, several hypotheses have been proposed and used in the past. One simpler alternative is to define the bond stress – slip relationship with linear branches [15]. Nevertheless, alternatively, a more robust non-linear relationship between bond stress and slip can be used. The relationship established by Eligehausen [15] and afterwards adopted by the Model Code 2010 [27] is expressed by the following non-linear functions as follows:

$$\tau = \tau_{max}\left(s/s_1\right)^{\alpha}; 0 \le s \le s_1 \quad (2)$$

$$\tau = \tau_{max}; s_1 \le s \le s_2 \quad (3)$$

$$\tau = \tau_{max} - \left(\tau_{max} - \tau_f\right)\cdot\frac{\left(s - s_2\right)}{\left(s_3 - s_2\right)}; s_2 \le s \le s_3 \quad (4)$$

$$\tau = \tau_f; s \ge s_3 \quad (5)$$

Fig. 6 depicts the bond stress – slip relationship according to [27]. Tab. 1 includes the parameters of the bond-slip relationship proposed by Model Code 2010 [27] for distinct bond conditions.

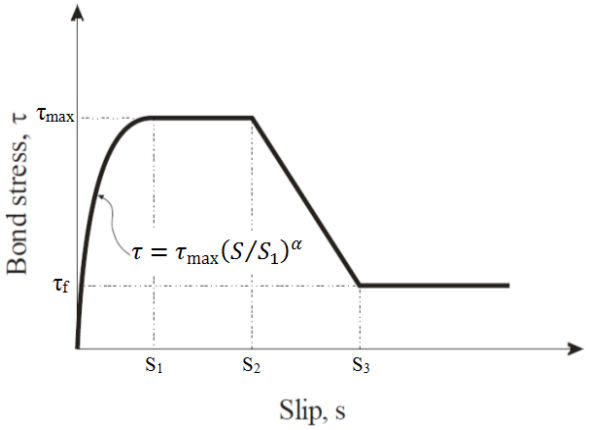

Figure 6: Local bond stress-slip law according to [27].

Bond Conditions	τ_{max}	τ_f	α [-]	s_1 [mm]	s_2 [mm]	s_3 [mm]
Good	$2.5(fcm)^{0.5}$	$0.4\tau_{max}$	0.4	1	3	Clear Rib spacing of rebar

Table 1: Parameters defining the bond-slip relationship [27].

In the present work two distinct local bond stress – slip laws were used. For the parametric study, the bond stress – slip relationship was modelled using the linear cohesive law provide by ABAQUS software, as depicted in Fig. 7. This constitutive model available in ABAQUS was originally developed for the delamination of composites, but it can also be used to model cohesion between steel rebar and concrete, assuming that the interaction between concrete and steel rebar can be collapsed to zero-thickness surface. This approach has been already previously adopted by Alfano and Serpieri [28,

29]. In a second stage, a similar local bond stress – slip law to that proposed by [27] was also used. In order to implement it in the software, it was needed to perform previously a transformation of the bond stress – slip law to a damage – slip relationship.

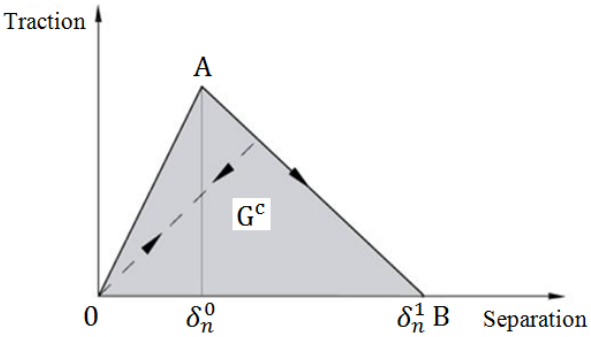

Figure 7: Linear bond-slip law [26].

With reference to the Fig. 7, the first part of the constitutive law is linear elastic up to the maximum bond stress (point A), involving an initial displacement δ_n^0. At this point the interface starts to become damaged. Once the maximum bond stress is reached and the crack begins to propagate, the stress starts to reduce up to the maximum displacement δ_n^1 (point B). G^c is the fracture energy needed to propagate the interfacial crack.

Concrete and steel constitutive behaviour

Regarding the mechanical behaviour of the steel rebar, it was assumed an elastic perfectly-plastic behaviour. On the other hand, to model the concrete behaviour two distinct approaches with different levels of complexity were adopted. It was assumed a linear elastic behaviour and nonlinear behaviour by using the Concrete Damage Plasticity (CDP) model comprised in the ABAQUS software [26]. The CDP model from the ABAQUS library [26] considers the total strain decomposed into an elastic (ε^{el}) and plastic (ε^{pl}) strain components, $\varepsilon = \varepsilon^{el} + \varepsilon^{pl}$. The stress-strain relation associated with the damage evolution is given by:

$$\underline{\sigma} = (1-d)\,\underline{D}_0^{el}\left(\underline{\varepsilon} - \underline{\varepsilon}^{pl}\right) \tag{6}$$

where d is the damage variable ($d = 0$ no damage, $d = 1$ fully damaged) and D_0^{el} is the non-damaged elastic modulus. Damage is associated with the typical degradation mechanisms of concrete – cracking in tension and crushing in compression, which involves a decrease of the elastic modulus. Damage is governed by the hardening variables $\tilde{\varepsilon}^{pl}$ and the effective stress $d = d\left(\bar{\sigma}, \tilde{\varepsilon}^{pl}\right)$. The hardening variables under compression ($\tilde{\varepsilon}_c^{pl}$) and tension ($\tilde{\varepsilon}_t^{pl}$) are considered independently.

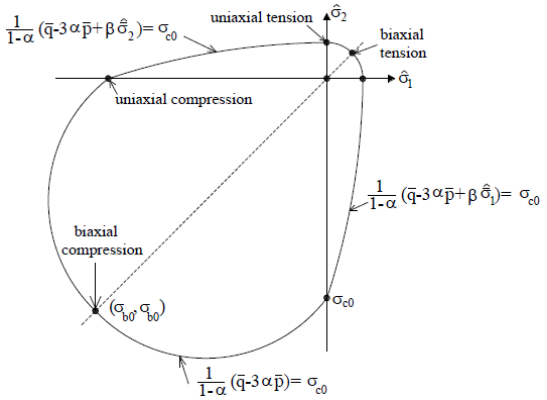

Figure 8: Yield surface of DCP model [26].

The adopted CDP model used a yield surface that was defined as the loading function proposed by Lubliner *et al.* [30], see Fig. 8. The evaluation of the yield surface was controlled by the two hardening variables, namely, the plastic strain in tension ($\tilde{\varepsilon}_t^{pl}$) and the plastic strain in compression ($\tilde{\varepsilon}_c^{pl}$).

Tab. 2 includes the mechanical properties of concrete and steel used in the numerical simulations. Regarding the steel tensile behaviour an elastic – perfectly plastic relationship δ_n^1 was considered with a yield stress of 567 MPa. On the other hand, Tab. 3 includes the constitutive parameters of the CDP model used to simulate the nonlinear behaviour of concrete when considered.

Material	Density, ϱ [kg/m³]	Young Modulus, E [GPa]	Poisson ratio, ν [-]
Steel	7800	200	0.30
Concrete	2400	30	0.20

Table 2: Mechanical properties adopted in the numerical simulations.

Dilatation angle [º]	Eccentricity [-]	σ_{bo}/σ_{co} [-]	Kc [-]
40.0	0.1	1.16	0.667

Table 3: The constitutive parameters of CDP model.

PARAMETRIC STUDY

This section presents the parametric study that was carried out to calibrate the numerical model for the pullout tests. This study evolves the analysis of the influence of distinct parameters on the numerical responses, such as: the mesh refinement, the cohesive element thickness and the viscosity coefficient.

Mesh refinement

To analyse the influence of the mesh refinement, it was considered in a first stage a linear elastic behaviour for concrete. For the interface behaviour it was used the relationship depicted in Fig. 7. For this task, four meshes similar to the one presented in Fig. 4 were considered. Tab. 4 presents several parameters for mesh characterization, such as number of elements and nodes, and respective computational time for completing the numerical simulation of the pullout test.

Mesh	Element quantity	Nodes quantity	Computational Time
1	2100	2790	48min 21s
2	3100	3945	49min 10s
3	4100	5100	61min 21s

Table 4: Mesh parameters.

The parameters to define the behaviour of the cohesive elements layer in terms of nominal stresses are presented in Tab. 5. The adopted damage evolution was of the type displacement with linear softening and maximum degradation. Moreover, two values for displacement at failure, namely, 5 and 1000 mm were adopted. In the last case, it corresponds practically to assuming no degradation of the bond stresses with the increment of slip.

Nominal Stress Normal-only Mode [MPa]	Nominal Stress First Direction [MPa]	Nominal Stress Second Direction [MPa]
0	10.26	0

Table 5: Nominal Stress.

Fig. 9 and 10 depict the results obtained in the numerical simulations considering an elastic behaviour for concrete and the local bond stress – slip relationship defined by Fig. 7 for the interface elements behaviour. As it was expectable the

ultimate slip obtained during pullout was almost 5 mm and 1000 mm, Fig. 9 and 10, respectively. In Fig. 10 it was opted to depict only the load - slip relationship up to a slip of 1 mm, nevertheless the pullout load kept constant practically up to the ultimate displacement (1000 mm). In both simulations, and excluding Mesh 1, the maximum pullout load was reached approximately for a slip of 0.2 mm, and the value was of 63.9 and 66.3 kN for the simulations carried out with and without bond stress degradation with slip, i.e. with an ultimate local slip of 5 and 1000 mm, respectively. Considering no degradation of the bond, stress increased in nearby 5% de maximum pullout load.

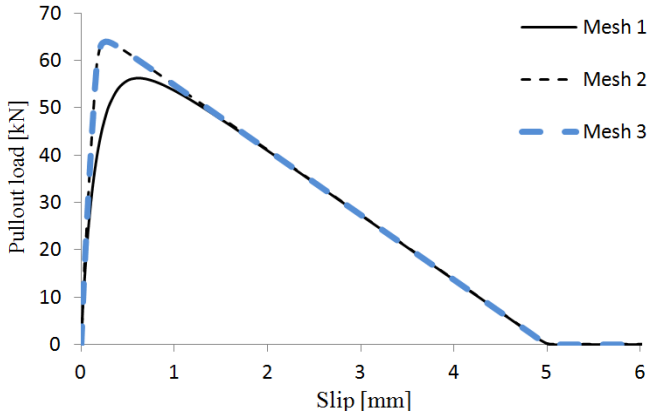

Figure 9: Pullout load - slip relationship with a 5 mm displacement at failure.

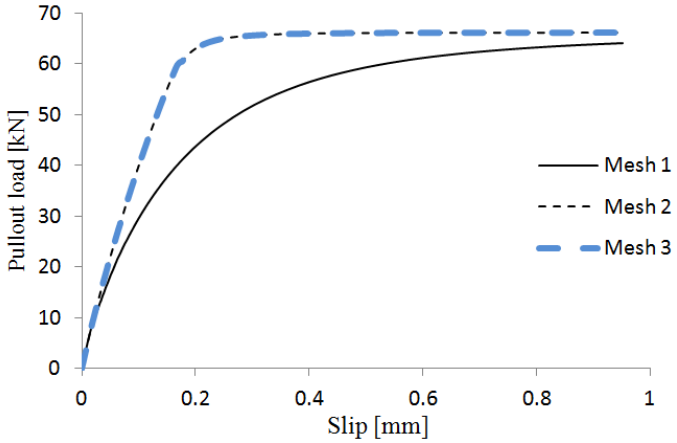

Figure 10: Pullout load - slip relationship with a 1000 mm displacement at failure.

After carrying out the simulations considering an elastic behaviour of the concrete surrounding the rebar, it was assessed the influence of the mesh refinement when using the Concrete Damage Plasticity model to model the surrounding concrete behaviour. For this purpose, three meshes were used, in particular, Mesh 3 and 4 that were the same used in the simulations when considering an elastic behaviour for concrete, and another mesh with a higher refinement in the rebar zone and a coarser refinement in the concrete farther from the interface zone. Regarding the interface cohesive behaviour, the adopted damage evolution also was of the type displacement with linear softening and maximum degradation. The value of displacement at failure was 5 mm. Tab. 6 includes the number of nodes and elements, as well as the computational time for completing the simulation of the pullout test.

Mesh	Element quantity	Nodes quantity	Computational Time
3	4100	5100	3h 36min
4	21960	25010	51h 40min
5	20500	24580	29h 46min

Table 6: Mesh parameters.

Fig. 11 presents the results obtained for the three meshes when considering the Concrete Damage Plasticity model. As it was expectable the maximum slip was 5 mm. In terms of maximum slip the results are similar to the ones obtained considering an elastic behaviour for concrete. As it is visible in Fig. 11 b), it was verified a sharper peak in meshes 3 and 5, which incremented nearby 3% the peak load. Based in this analysis it was adopted Mesh 4, to carry out the forthcoming analysis.

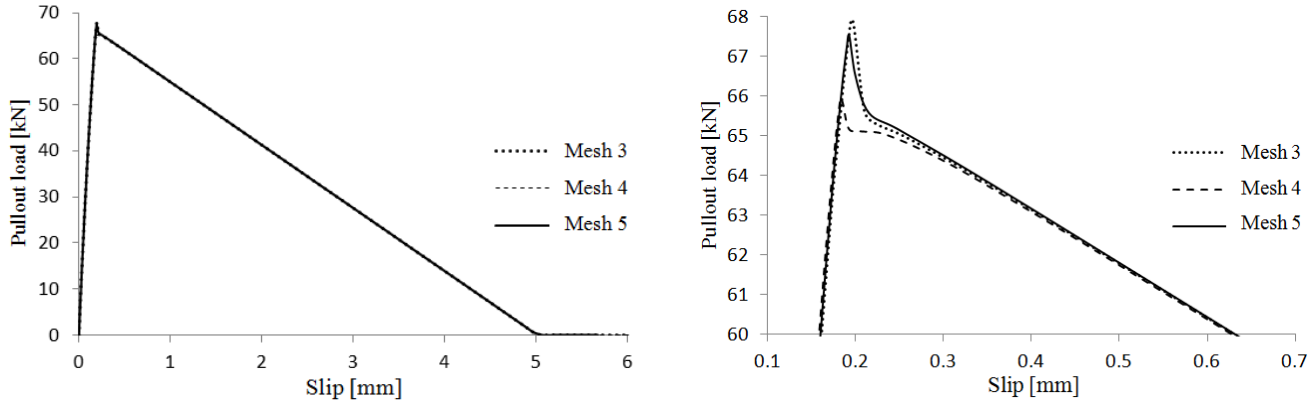

Figure 11: Bond stress-slip relationship displacement at failure equal to 5 mm: a) complete curve; b) detail peak curve.

Cohesive element thickness

The interface was simulated with the use of cohesive elements in-between the rebar and surrounding concrete. Since these are not pure interface elements, a certain thickness must be ascribed to the element. The cohesive element's thickness used in the parametric study were 0.1, 0.5 and 1.0 mm, respectively. Fig. 12 and 13 show the results for the three thicknesses, adopting an ultimate slip of 5 and 1000 mm, respectively. As foreseeable, with the thickness increase was verified an increase of the maximum pullout load. This occurs because the cohesive elements' mid surface is farther from the rebar's surface, consequently, there is an increase of the interface area. Therefore for the same bond stress profile it will result in higher shear stresses at the interface and consequently a higher pullout load.

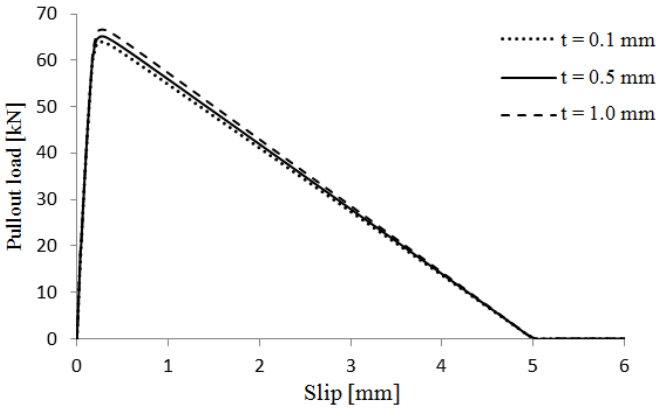

Figure 12: Bond stress-slip relationship displacement at failure equal to 5 mm, with different thickness of cohesive elements.

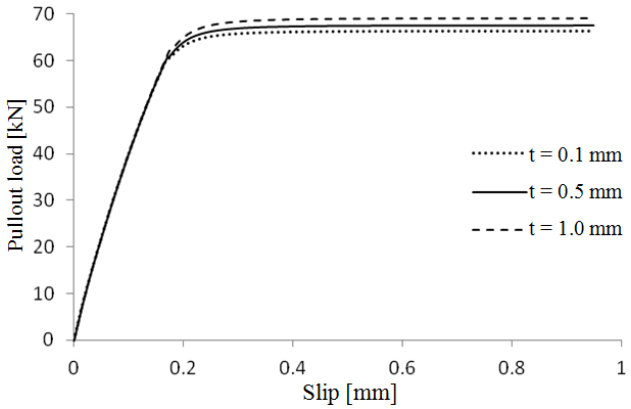

Figure 13: Bond stress-slip relationship displacement at failure equal to 1000 mm, with different thickness of cohesive elements.

Viscosity coefficient

The viscosity coefficient is a regularization parameter for obtaining convergence in damage models that exhibit a softening response. It allows the analysis to converge after the peak load is attained, but the results can be unrealistic if a proper value is not selected. The influence of the viscosity in the pullout response was carried out. For this purpose three quite distinct values for the viscosity coefficient, namely, 0.001, 0.0001 and 0.00001 were selected. These analyses were carried out for two linear bond stress – slip relationships, adopting an ultimate slip of 5 and 1000 mm, respectively. As it can be observed in Fig. 14, for the local bond law defined with an ultimate slip of 5 mm, the viscosity coefficient only does not

have influence if a quite small value is adopted, i.e. equal to 0.00001. For a viscosity value of 0.001 the results were completely incoherent, with the maximum pullout load attaining the value of 200 kN, approximately three times the real value. Fig. 15 shows the results adopting a bond stress – slip law with an ultimate slip of 1000 mm. In the latter case, the viscosity coefficient only has influence for the higher viscosity value, i.e. 0.001, causing an increasing in maximum pullout load of approximate 10%. Based on these results, it was decided to use the smallest viscosity coefficient in all simulations (0.00001), this option leads to an increase of the computational time cost.

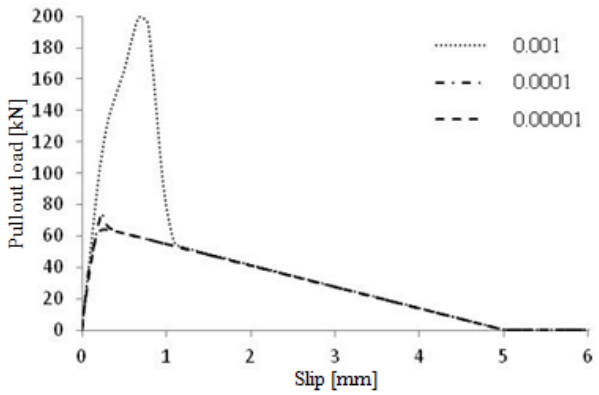

Figure 14: Bond stress-slip relationship displacement at failure equal to 5 mm simulated with different viscosity coefficients.

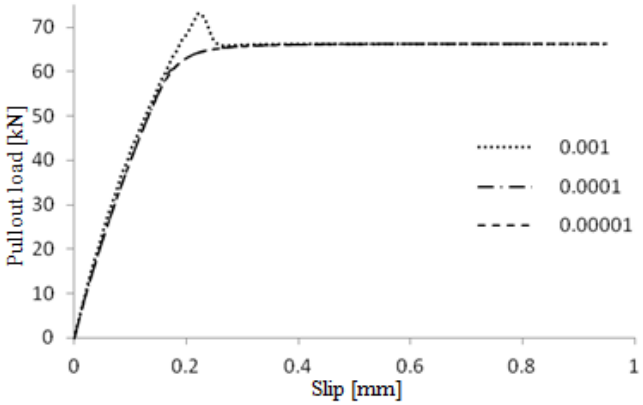

Figure 15: Bond stress-slip relationship displacement at failure equal to 1000 mm simulated with different viscosity coefficients.

NUMERICAL MODELLING OF THE SENA ET AL. (2009) PULLOUT TESTS

This section presents the numerical results within the finite element framework regarding the simulation of the experimental pullout tests performed by Sena-Cruz *et al.* [31].

Smooth rebar model

The simulations were firstly performed assuming a smooth surface for the steel rebar. The pullout behaviour of three types of rebars, namely, non-alloy, galvanized and galvanized + epoxy rebar were modelled. The obtained numerical results were compared with the experimental results and with the results obtained using the analytical model proposed by Sena-Cruz *et al.* [31]. Tab. 7 includes the parameters that define the local bond – slip law (Fig. 6) used in the numerical simulations. These parameters were obtained by an inverse analysis procedure using an analytical shear-lag model [31]. The inverse analysis procedure consisted in fitting the numerical pullout force – slip relationship with the experimental correspondent one by varying the local bond law parameters. In these simulations the FE mesh depicted in Fig. 1 was used.

Rebar	τ_{max}	α [-]	s_1 [mm]	Error [%]
Galvanized + epoxy	$0.73\ (fcm)^{0.5}$	0.4	2.00	3.9
Galvanized	$1.46(fcm)^{0.5}$	0.62	1.30	2.5
Non-alloy	$1.75(fcm)^{0.5}$	0.52	1.30	1.8

Table 7: Parameters of the bond-slip relationship obtained by inverse analysis [31].

Fig. 16 depicts both the experimental and numerical results from the finite element analysis, for specimens with non-alloy steel rebars, in terms of pullout force *vs.* slip. The numerical results were inside of experimental envelope obtained experimentally, however the simulations results by ABAQUS slightly overestimates the results obtained by the analytical formulation of [31], in terms of stiffness and maximum pullout force.

Numerical results of the specimens with galvanized steel rebars are presented in Fig. 17. The numerical results are also inside of experimental envelope, except in initial zone of slip, were the simulations results by ABAQUS are a little outside of envelope. In terms of stiffness and maximum pullout force, the conclusions are similar to obtained with the non-alloy rebars. The response of ABAQUS has an initial peak of the pullout force followed by a softening, afterwards it was observed an increase of the pullout force.

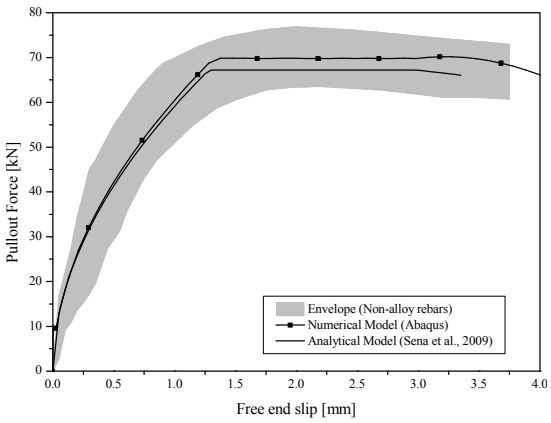

Figure 16: Numerical simulation of the experimental pullout curves (non-alloy rebar).

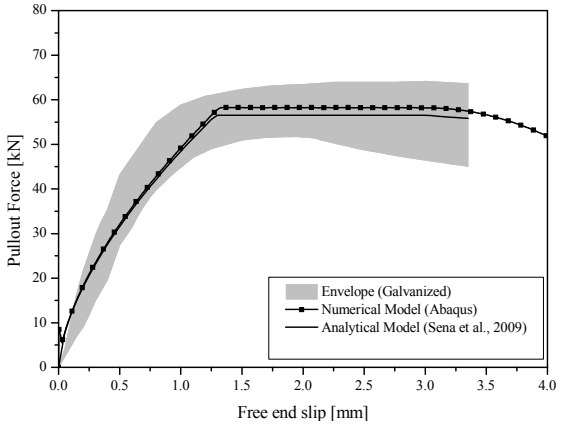

Figure 17: Numerical simulation of the experimental pullout curves (galvanized rebar).

Numerical results for galvanized + epoxy rebar, presented in Fig. 18, are similar to the ones obtained with galvanized rebars. But it is possible to see that experimental results also present an initial peak of pullout force followed by a softening, after the increase of the pullout force.

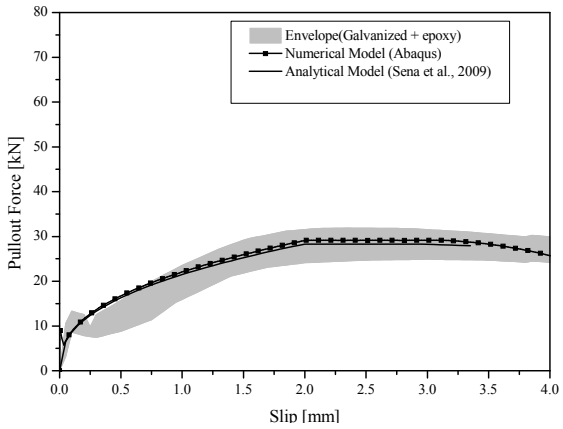

Figure 18: Numerical simulation of the experimental pullout curves (galvanized+epoxy rebar).

Model with the rebar's ribbing

In this section the pullout tests [31] were modelled using the geometrical representation of the rebars' ribbs. Note that an approximate geometry was adopted due to the complexity of the real rebar ribs geometry. Fig. 4 depicts schematically the adopted mesh, which included 8 ribbs along the embedded length of the steel rebar in the concrete. Three different heights of ribbing were considered in the three distinct simulations that were carried out, respectively, 0.20, 0.26 and 0.30 mm. The ribs allowed to simulate the mechanical reinforcement mechanism due to the rib interlock verified between concrete and ribbing in experimental test. Moreover, the cohesive elements were used to simulate the effects of steel-concrete chemical adhesion and frictional shear. In these simulations the parameters that defined the behaviour of the cohesive elements layer, in terms of nominal stress, are presented in Tab. 8.

Fig. 19 depicts the pullout force *vs.* free-end slip relationships for the performed numerical simulations. The results that better agreed with the experimental results were obtained with a ribbing height of 0.26 mm, where the maximum pullout force obtained in the numerical simulation was similar to the experimental. The stiffness of the numerical response was higher than the one of the experimental results. The horizontal plateau of the pullout force *vs.* slip curve was not possible to reproduce numerically. Instead, the softening verified numerically was very pronounced.

The abovementioned differences observed between the numerical results and experimental results could be ascribed to several factors. First of all, note that the geometric representation of the ribs was approximate, since the actual ribs geometry is quite complex and its disposition along the rebar's surface is non uniform. Therefore for modelling accurately the ribs geometry a more complex and full 3D geometrical model should be developed, in which the axisymmetric stress state cannot be considered. As previously stated the numerical responses with the discretization of the ribs were stiffer than the experimental pullout behaviour. To the latter fact may contributed the disposition of the interface elements along the lateral inclined faces of the ribs, which are not submitted to a pure fracture mode II, since they are also subjected to compressive stresses that will increase the confinement level. This aspect may contributed to an increase of the response stiffness. On the other hand, the steeper softening decay observed in the numerical curves may be related to adopted geometry of the ribs within the numerical model. In the numerical model, the start of the softening stage, after the peak load, coincides with the plastification of the compressive bulk wedges formed in front of the ribs during the pullout procedure, and the increase of the relative displacement between ribs and the surrounding concrete.

Nominal Stress Normal-only Mode [MPa]	Nominal Stress First Direction [MPa]	Nominal Stress Second Direction [MPa]
0	0.63	0

Table 8: Nominal stress.

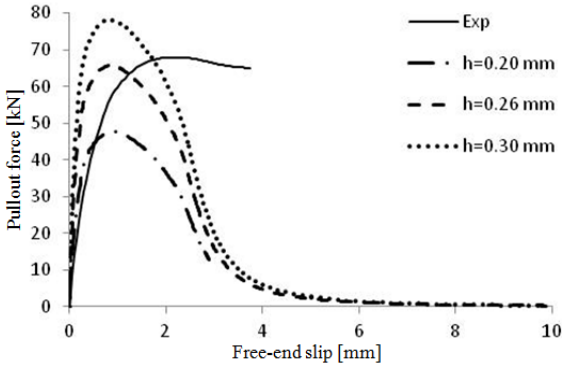

Figure 19: Numerical simulation of the experimental pullout curves (rebars with ribs).

CONCLUSIONS

With the aim of studying the bond behaviour between galvanized rebars and concrete in pullout tests, distinct numerical simulations were carried out using the finite element method framework. A parametric study of the main numerical variables was performed, also to calibrate the model. The numerical simulations of the pullout tests carried out by [31] were compared with both the experimental results and the simulations with an analytical shear-lag model. Using the same bond stress – slip relationships the results obtained by the finite element method rendered a higher stiffness and maximum pullout load when compared to ones obtained with the analytical model by [31]. The pullout tests were successfully modelled assuming the steel rebar as smooth, as long a proper local bond stress – slip law is adopted. The numerical simulations including in the geometric model the rebar ribbings, at this stage dis not render so good results and further research should be carried out. The differences observed between the numerical results and experimental results when the ribs were modelled, could be ascribed to the approximate geometric representation of the ribs. Therefore for modelling accurately the ribs geometry a more complex and full 3D geometrical model should be developed, in which the axisymmetric stress state cannot be considered. Moreover, since some interface elements were not subjected to a pure fracture mode II, they may also contribute to a stiffening of the initial numerical pullout response.

REFERENCES

[1] Considère, M., Influence des armatures métalliques sur les proprietes des mortiers e bétons, Le Béton Armé, 9 (1899).

[2] Considère, M., Influence des armatures métalliques sur les proprietes des mortiers e bétons, Le Béton Armé, 10 (1899).
[3] Talbot, A. N., Tests of concrete I. Shear II. Bond, University of Illinois Bulletin, IV (1906)
[4] Webb, R., Wilsey, G. H., Bonding strength of concrete and steel, Armour Institute of Technology, (1908).
[5] Emin, G. H., Laskey, H., Tobias, W. R., Bond stress of lap reinforced concrete beams, Armour Institute of Technology, (1911).
[6] Abrams, D. A., Test of bond between concrete and steel, University of Illinois Bulletin, XI (1913).
[7] Rehm, G., The fundamental law of bond, In: Proceeding of the Symposium on bond and Crack Formation in Reinforced Concrete, Stockholm; RELIM, Paris, (1957).
[8] Rehm, G., The basic principle of bond between steel and concrete, Deustcher Ausschuss fur Stalbeton; Wilhelm Ernest and Sohn, Berlin, 138 (1961)
[9] Goto, Y., Cracks formed in concrete around tension bars, ACI Journal, 68(4) (1971) 244-251.
[10] Tassios, T.P., Properties of bond between concrete and steel under load cycles idealizing sismic actions, Comité Euro-international Du Béton, Paris, 131 (1979).
[11] Tepfers, R., Cracking of concrete cover along anchored deformed reinforcing bars, Magazine of Concrete Research, 31(106) (1979) 3-11.
[12] Stanton, J. F., McNiven, H. D., The development of a mathematical model to predict the flexural response of reinforced concrete beams to cyclic loads, EERC report, University of California, Berkeley, 79-2 (1979).
[13] Ciampi, V., Eligehausen, R., Bertero, V. V., Popov, E.P., Analytical model for concrete anchorages of reinforcing bars under generalized excitations, Earthquake Eng. Res. Center, University of California, Berkeley, 82/23 (1982) 121.
[14] Hawkins, N. M., Lin I.J., F.L. Jeang, Local bond strength of concrete for cyclic reversed loadings, Bond in Concrete, P. Bartos (editor), Applied Science Publishers Ltd., London, (1982) 151-161.
[15] Eligehausen, R., Popov, E.P., Bertero, V.V., Local bond stress-slip relationships of deformed bars under generalized excitation, University of California; National Science Foundation, UCB/EERC-83/23 (1983).
[16] Darwin, D., Development length criteria for conventional and high relative rib area reinforcing bars, ACI Structural Journal, Farmington Hills, 93(3) (1992) 709-720.
[17] Gambarova, P.G., Rosati, G.P., Bond and splitting in bar pull-out: behavioural laws and concrete cover role, Magazine de Concrete Research, 49(179) (1997) 99-110.
[18] Sener, S., Bazant, Z.P., Becq-Giraudon, E., Size effect on failure of bond splices of steel bars in concrete beams, ASCE – Journal of Structural Engineering, 125(6) (1999) 653-660.
[19] Kayali, O., Yeomans, S. R., Bond of ribbed galvanized reinforcing steel in concrete, Cement & Concrete Composites 22 (2000) 459-467.
[20] Li, C. Y., Finite Element Simulations of fiber pullout toughening in fiber reinforced cement based composites, Advanced Cement Based Materials, 7 (1998) 123-132.
[21] Lettow, S., The simulation of bond between concrete and reinforcement in nonlinear three-dimensional finite element analysis, In: 5th International PhD Symposium in Civil Engineering, Delft, The Netherlands, (2004).
[22] Torres, L., Baena, M., Turon, A., Cahís, X., Barris, C., Simulation of bond behaviour between fiber reinforced polymer bars and concrete, In: 8th International Symposium on Fiber Reinforced Polymer Reinforcement for Concrete Structures, Patras, Greece, (2007).
[23] Shafaie, J., Hosseini, A., Marefat, M. S., 3D finite element modelling of bond-slip between rebar and concrete in pull-out test, In: 3rd International Conference on Concrete & Development, Iran, (2009).
[24] Lowes, L.N., Finite element modelling of reinforced concrete beam-column bridge connections, Ph. D. Thesis, Civil Engineering Division, University of California, Berkeley, USA, (1999).
[25] Bond of reinforcement in concrete-state of the art report, Fib-Bulletin, Lausanne, 102000.
[26] ABAQUS version 6.11 User's manual. RI: Hibbitt, Karlsson & Sorensen Inc, (2011).
[27] Fédération internationale du béton / International Federation for Structural Concrete (fib), "FIP model code for concrete structures 2010", Paul Beverly, Lausanne, Switzerland, (2013).
[28] Alfano, G., Marfia, S., Sacco, E., A cohesive damage-friction interface model accounting for water pressure on crack propagation, Computer methods in applied mechanics and engineering, 196 (2006) 192-209.
[29] Serperi, R., Alfano, G., Bond-slip analysis via a thermodynamically consistent interface model combining interlocking, damage and friction, Int. J. Numer. Meth. Engng, 85 (2011) 164-186.
[30] Lubliner, J., Oliver, J., Oller, S., Oñate, E., A plastic-damage model for concrete, J. Solid structures, 25 (1989) 299-326.

[31] Sena-Cruz, J., Cunha, V.M.C.F., Camões, A., Barros, J.A.O., Cruz, P., Modelling of bond between galvanized steel rebars and concrete, In: Congresso de Métodos Numéricos en Ingenieria, Barcelona, Spain, (2009) 20.